ADVANCED FUNCTIONAL MATERIALS
www.afm-journal.de

Hierarchical Weaving Metafabric for Unidirectional Water Transportation and Evaporative Cooling

Ling Zhang, Yuwei Guo, Ruolian Mo, Xiang Liu, Guang Wang, Ronghui Wu, and Hongling Liu**

Smart apparel with unidirectional sweat transportation functionality is highly desirable for wearing comfort. However, simultaneously achieving fast unidirectional water transport, mechanical robustness, human body comfortability, and industrialized fabrication is challenging because of the difficulty in fiber-yarn-fabric multiscale textile structure manipulation. Here, for the first time, a unidirectional water-transportation metafabric (UWTM) with hierarchical weft-double-weave structure is developed using industrial-producible weaving technology. The UWTM not only shows a fast unidirectional sweat transportation property, but also a robust mechanical property, air permeability, tailorability, and human body comfortability. The unidirectional water transportation is realized by a well-engineered wettability gradient along fabric thickness direction by two-set weft yarns and one-set warp yarn. The UWTM shows a strong one-way transport capacity of 984%, with a short water droplet transportation time of 4 s. In addition, the unidirectional water transportation leads to an evaporative cooling effect to the human body, resulting in a 1.6 °C cooling compared with the most used cotton fabrics, exhibiting excellent wet-heat transfer responsiveness, and ensuring a comfortable microclimate between human skin and the environment. The facile and scalable method presented here paves a way for the design of fluorine-free, robust, comfortable, and wearable unidirectional water transport fabrics.

1. Introduction

Smart textiles with the functionality of maintaining the physiological comfort of the human body are acute, especially in extreme environmental conditions such as those faced by athletes, soldiers, or industrial workers.[1] Evidently, moisture wicking property of textiles plays a most important role due to their capability of providing a drier and cooler microclimate between human body and textiles.[2] It requires programmable structures through architected design of yarn hydrophilicity, diameter, and relative density for microfluidic control. Traditional sweat wicking textiles normally either use only hydrophilic or hydrophobic materials. Hydrophilic fabrics, such as cotton can adsorb the sweat from the human skin very easily, but they will stay there until they dried, resulting in undesired wet sticky or cold sensations.[3] Hydrophobic fabrics such as Coolmax with profiled cross section was recognized as an attractive strategy because it exerts the innate ability of quick drying due to its moderately hydrophobic and increased surface area.[4] However, the moisture-wicking process in such fabrics remains bidirectional; that is, it can be triggered from the skin to the environment as well as the opposite direction, which will limit its practical applications at a high humidity level or after a passing rain shower.

To solve the aforementioned problems, developing fabrics with unidirectional water transport is of great importance. Current research on directional water transport can be roughly divided into two categories, nonwoven fabrics[1c] and post-treated woven fabrics.[1a] Nonwoven fabrics by assembling micro- and nanofiber films have been demonstrated to show good antigravity directional water transportation.[5] However, such nonwovens generally exhibit poor mechanical properties, which restrict their applications in wearable textiles.[6] Post-treated woven fabrics with asymmetric structure are mostly produced by post fabric finishing process based on the weaved fabric.[7] Specifically, Zeng et al. reported a fabric with directional water transport capability by single-sided electrospray coating of hydrophilic fabrics with hydrophobic resins.[1a] More recently, Wang et al.[8] used a hydrophobic finishing agent in a two-step electrospray of hydrophilic cotton woven fabrics with asymmetric wetting

L. Zhang, Y. Guo, R. Mo, X. Liu, G. Wang, R. Wu, H. Liu
Key Laboratory of Textile Science and Technology
Ministry of Education
College of Textiles
Donghua University
Shanghai 201620, China
E-mail: ronghuiwu@uchicago.edu; hlliu@dhu.edu.cn
R. Wu
Pritzker School of Molecular Engineer
University of Chicago
Chicago 60637, USA

The ORCID identification number(s) for the author(s) of this article can be found under https://doi.org/10.1002/adfm.202307590

DOI: 10.1002/adfm.202307590

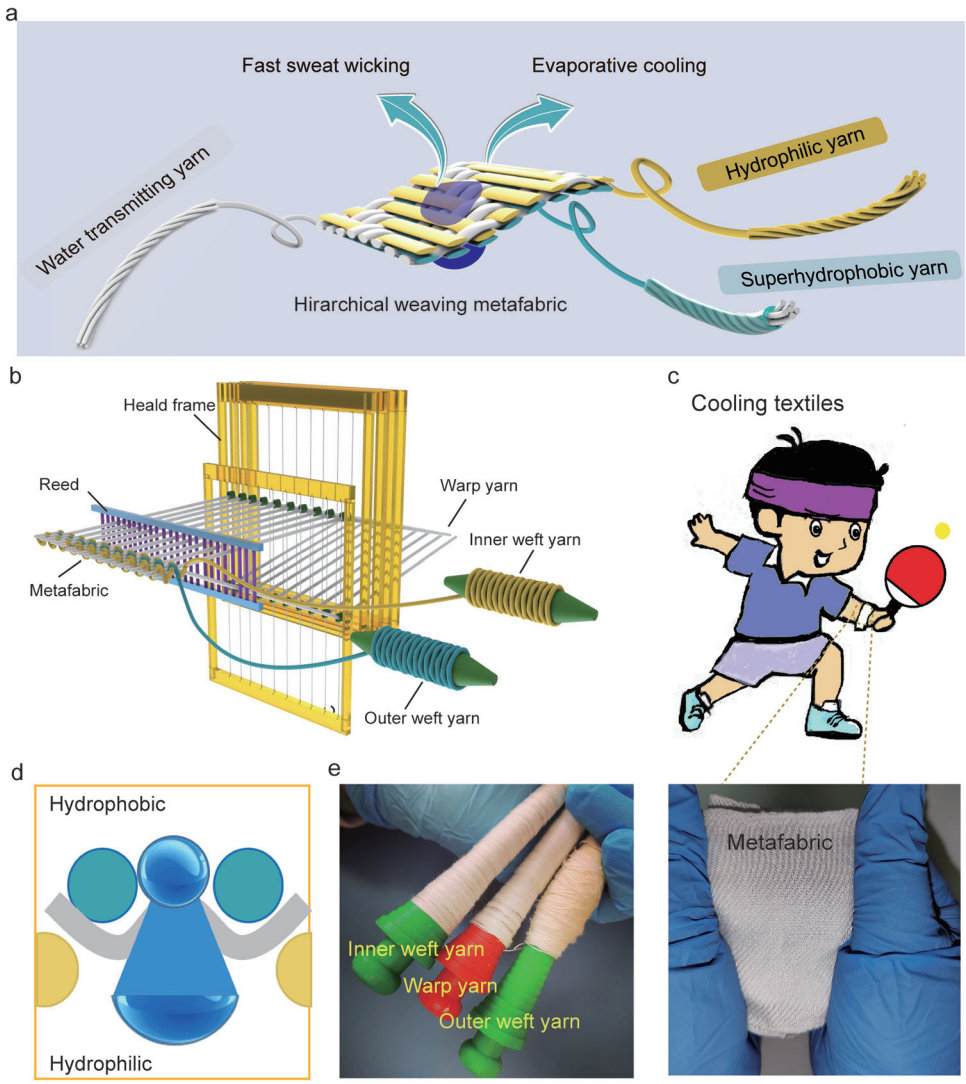

Figure 1. Unidirectional water-transportation metafabric for unidirectional sweat transportation and evaporative cooling. a) Architecture of UWTM. It is composed of superhydrophobic outer weft yarn, hydrophilic inner weft yarn, and hydrophobic warp yarn. b) Fabrication process of UWTM using low-cost, continuous, and mass-productive weaving technique. c) Optical image of UWTM fabricated by the double weft weaving technology and its application potentials in exercise clothes. d) Unidirectional sweat transportation from the hydrophobic side to the hydrophilic side. e) Bobbins of the three yarns for UWTM weaving.

structure and reported the high permeability one-way water transport (OWT) performance. However, finishing agents used for surface functionalization of these woven fabrics are mostly fluorinated substances or toxic solvents,[9] which could cause environmental pollution and health problems. More important, weaved fabric coating will sacrifice the air permeability, flexibility, washability, wearing comfort, and abrasion resistance of fabrics, which is critical for wearable textiles. Therefore, a novel method for weaving textiles design for unidirectional water-transportation needs to be developed.

Here, for the first time, a novel unidirectional water-transportation metafabric (UWTM) with hierarchical structure and robust mechanical property is developed using an industrial-producible weaving technique. Three fabric structures, 2D satin-weave, double-weft–weave, and stitching-double–weave are designed and systematically studied for optimization of the water-transportation capacity. The UWTM with weft-double–weave structure is composed of one set of warp yarn and two sets of weft yarns, forming an asymmetric wettability gradient, that is, superhydrophobic outer weft yarns (SOWY), water-transportation warp yarns (WTWY), and hydrophilic inner weft yarns (HIWY) (**Figure 1**a). A fluorine-free superhydrophobic finishing is introduced on polyester (PET) by hierarchical crosslinking for the SOWY, while viscose fibers with microgrooves are chosen for the HIWY, and polyester fibers with low moisture adsorption are used for the WTWY. Owing to the unique hierarchical structure, UWTM shows a fast water transportation speed from the skin to the outer environment, keeping a dry and cool microclimate between the textile and human body. In addition, for better understanding the unidirectional water transportation mechanism, the moisture management performance of UWTM was theoretically and experimentally analyzed. Besides, the excellent

mechanical properties, weavability, air permeability have been discovered and discussed. Moreover, the sweat-wicking property of UWTM is further demonstrated to accelerate the body cooling via evaporation. The performance compared with traditional textiles, such as cotton and PET has been conducted. The UWTM provides wide application prospects in perspiration and personal thermoregulation.

2. Results and Discussion

2.1. UWTM Structure Design and Fiber Wettability Engineering

UWTM is fabricated using a continuous, mass-productive, and low-cost weaving technology with two sets of weft yarns and one set of warp yarn, as shown in Figure 1a,b; Figure S1 and Video S1, Supporting Information. In the UWTM, superhydrophobic inner weft yarns (SOWY) and hydrophilic outer weft yarns (HIWY), are interlaced with the WTWY alternatively, forming an asymmetric wettability gradient along the fabric thickness direction. Two sets of weft yarns are regularly fed into the loom and interlaced with warp yarns. The well-controllable textile patterns with governable yarn trajectory are realized by computer regulated weft yarn lifting plan. Moreover, to enhance the unidirectional water transportation ability, hydrophilic yarn is interlaced into the superhydrophobic side every two weaving cycles at intervals. When sweat is on a hydrophobic layer, droplets can penetrate through these hydrophilic yarns quickly, break the surrounding meniscus and decrease the Laplace pressure. As the most commonly used synthesis fiber, PET fibers are chosen as raw materials for SOWY and WTWY because of its mass productivity, robust mechanical property, and durability. Hydrophobic grafting and multi-scale roughness is further applied to PET yarns to realize the superhydrophobic yarns for SOWY. Meanwhile, grooved viscose fibers are chosen for WTWY because of its excellent hydrophilicity and good wearing comfort. With precise design, the unique fiber-yarn–fabric multiscale textile with double-weft weaving structure enables water droplet to penetrate from the bottom hydrophobic layer to the top hydrophilic fabric surface owing to capillary force. When people wear the UWTM exercise or move in hot weather and get sweat, the unique fabric design will drive the perspiration to be transported and diffused into the outer hydrophilic fabric surface, maintaining a dry and cool body-textile microclimate to ensure the wearing comfort, as shown in Figure 1c,d. As the weaving technology weave the functional yarns into a metafabric continuously without any post-treatment process (Figure 1e and Figure S2, Supporting Information), UWTM also have excellent mechanical property, flexibility, stretchability, breathability, conformity, and tailorability, which is indispensable but easily neglected in functional and smart textile research.

To guarantee an excellent performance for UWTM, the asymmetric wettability gradient design of yarns was dominant. Here, a fluoride-free bifunctional copolymer was strongly bonded on the PET fiber surfaces to achieve the superhydrophobic yarn for SOWY. The copolymer is synthesized by solvothermal copolymerization using *N*,*N*-ethylenebisacrylamide (MBAA) and divinylbenzene (DVB), denoted as co-MBAA-DVB, as shown in **Figure 2**a,b and Figure S3, Supporting Information, and Experimental Section. Co-MBAA-DVB has a hierarchical porosity with multi-scale surface roughness, as shown in the N_2 adsorption isotherm and scanning electron microscopy (SEM) images in Figure S4, Supporting Information. Considering polydimethylsiloxane (PDMS) owns low surface tension and good permeability, it is used to penetrate the porous structure to design micro or nano interface on PET yarn. A bifunctional copolymer network is constructed by combining diacrylamide groups with medium aromatic chains on the PDMS substrate during yarn finishing process. Moreover, methyl-2-cyanoacrylate (MCA) is used to form a strong and durable coating on the surface of polyester yarn owing to the synergistic crosslinking effect of PDMS and MCA. The polymerization of MCA was completed in a few seconds with the water vapor in the air mainly acting as a nucleophilic reagent (nu-). The C—C and C—O bonds on polyester are opened by high-energy particles to form C— and O— active sites, which lead to free radical polymerization with PDMS on the surface, resulting in stable and solid grafting of the hydrophobic film to the yarn surface. Furthermore, when the yarn was coated by PDMS, the diluted PDMS partly penetrated the interface between fibers and co-MBAA-DVB, and even inside the porous structure, enabling a strong adhesion. For MCA coating, due to the existence of ethyl acetate solution, the polymerization of MCA completed with the water vapor will be delayed, more conducive to form a cross-linked network to fix co-MBAA-DVB. Consequently, PDMS and MCA with co-MBAA-DVB on the polyester yarn could form stable interpenetrating polymer networks with low surface energy. After the coating treatment, a robust coating is firmly adhered to the substrate, showing abundant meso/macropores with a rough surface, which is similar to co-MBAA-DVB.

The compositions of co-MBAA-DVB and SOWY were identified by the ^{13}C NMR and FTIR investigation, as shown in Figure 2c,d. The ^{13}C NMR spectra of nanoporous polymer demonstrate signals at 127, 142.5, 145, 44, and 173.5 ppm. The signal at 127 ppm is attributed to C without substitution on the benzene ring. The signals at 142.5 and 145 ppm are from the signal of C at the para substitution in the benzene ring. The signal at 173.5pm is assigned to C in C═O in MBAA, and the signal at 44 ppm corresponds to C in fatty amines in the polymer. This indicated that DVB and MBAA were polymerized successfully. According to FTIR spectrum in Figure 2d, the SOWY gives additional peaks at 3390 and 1557 cm^{-1}, attributed to N—H stretching vibration and bending vibration of MBAA. In addition, the characteristic bands of polydivinylbenzene (PDVB) polymers observed at 1650 and 2960 cm^{-1} are ascribed to C═C and C—H stretching frequencies respectively, demonstrating the presence of PDVB-MBAA on the surface of coated yarn. Meanwhile, the C═O stretch occurred at 1740 and 1250 cm^{-1} from MCA, and the strong peaks of 798 and 1024 cm^{-1} corresponding to Si—C and Si—O—Si stretching from PDMS, which indicated the formation of the superhydrophobic coatings can be attributed to the synergistic cross-linking of MCA, PDMS, and MBAA&DVB.

After surface treatment, SOWY shows a superhydrophobic property with a high contact angle of 159.7° (Figure 2b). In addition, to check the uniform and full coating of the copolymer on fiber surface, different regions are randomly selected to be observed by SEM, as shown in Figure S5, Supporting Information. The SOWY fiber surface is fully covered by the organic species, which is indispensable to guarantee superhydrophobicity.

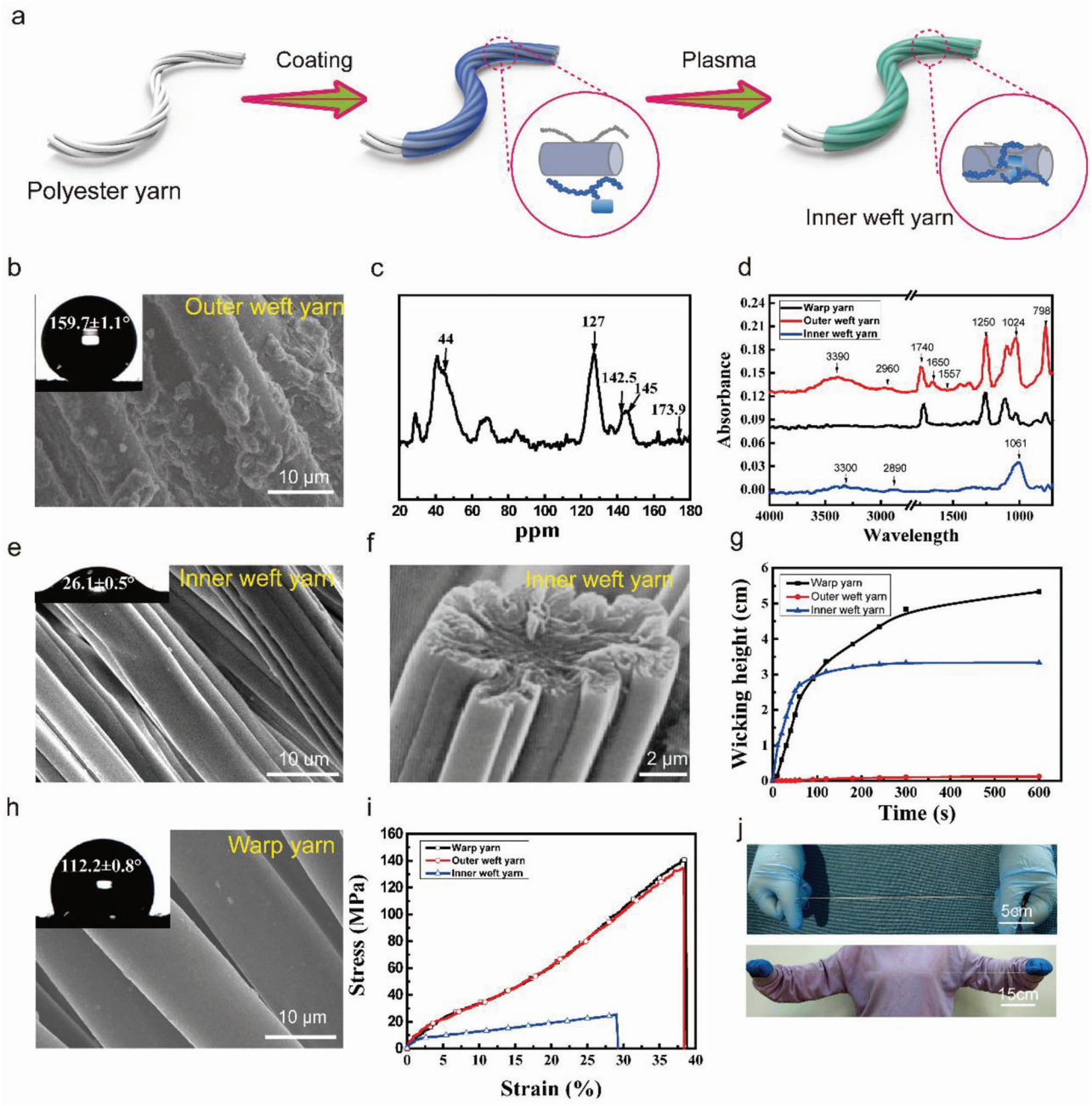

Figure 2. Fabrication, structure, wettability, and mechanical properties of weft warp yarns for UWTM. a) Fluoride-free surface treatment on polyester fibers for superhydrophobic outer weft yarns. b) Rough surface and large contact angle showing the superhydrophobicity of outer weft yarn. c) Nuclear magnetic resonance spectroscopy of outer weft yarns. d) FTIR spectrum of outer weft yarn, inner weft yarn, and warp yarn. e,f) Inner weft yarn made of viscose fibers with microgrooves on the surface, showing a small contact angle. g) Wicking height of the three yarns. Warp yarn shows a highest wicking height, which benefit the water transportation. h) Smooth surface and hydrophobicity of warp yarn. Outer weft yarn, warp yarn, and inner weft yarn show a contact angle gradient of 159.7°, 112.2°, and 26.1°, determining the unidirectional sweat transportation for UWTM. i) Stress–strain curves of three yarns, exhibiting a robust mechanical property for further UWTM weaving process. j) Optical image showing the flexibility and meter-scale productivity of superhydrophobic outer weft yarn.

To ensure the water adsorption on the upper side the textile, grooved viscose fibers with high hygroscopicity and hydrophilicity are chosen as the materials for HIWY. As shown in longitudinal and cross-sectional SEM images in Figure 2e,f, HIWY fiber exhibits a uniform microgroove structure, enhancing their specific surface area and grants the excellent wetting properties. As shown in the FTIR spectrum in Figure 2d, the absorption peak at 1016 cm^{-1} is caused by C—O stretching vibration, which is the characteristic absorption peak of cellulose. The wide and strong absorption peak at 3300–3450 cm^{-1} is caused by O—H

stretching vibration.[10] The large number of hydroxyl groups in the molecular chain confers it a good hygroscopicity. The viscose fibers are twisted into yarns and formed into axially continuous pores along the fiber directions, greatly enhancing the wicking effect. The wicking rate reached 15.4 mm min^{-1} for the viscose yarn in the first 2 min, which was higher than that of the modified cotton yarn (11.3 mm min^{-1}), WTWY, and SOWY (Figure 2g and Figure S5, Supporting Information). It is worth mentioning that because of the superhydrophobicity, SOWY offered almost 0 wicking effect after being immersed in blue ink simultaneously for 10 min. Therefore, viscose fibers in HIWY, which is on the top layer of the cloth, will quickly absorb the sweat penetrated from the hydrophobic layer (SOWY) and evaporate into the atmosphere, thereby effectively cooling down the human body.

For the water transportation yarn (WTWY), it needs to transfer water from the hydrophobic layer to the hydrophilic layer with a high speed, without water adsorption or storage. PET yarn which has both hydrophobicity and good wicking property, and low adsorption is perfect for the WTWY design. PET has a low water absorption of 0.4% because of its absence of hydrogen bonding sites.[11] As illustrated in Figure 2h, WTWY has a contact angle of 112.2°, showing a hydrophobic property. WTWY exhibits a significantly higher wicking speed (26.7 mm min^{-1}) and height (53 mm in 10 min) than the SOWY. Therefore, when the sweat stayed on the fiber surface, WTWY will not store the liquid, instead, it will transport the sweat from SOWY fibers to the HIWY fibers. During the process, the smooth surface of WTWY facilitates the water droplet transportation (Figure 2c). Based on the aforementioned discussion, the inner weft yarn, water-transportation warp yarn, and weft yarn form an excellent hydrophilicity enhancement gradient, which is highly desirable in the UWTM design.

Figure 2i shows the stress–strain curves of HIWY, SOWY, and WTWY. All these yarns show a robust mechanical property that can meet the weaving processing of textiles. During the weaving process, warps are held under high tension, moves up and down for shed formation. Therefore, it has a higher mechanical demand compared with weft yarns. In our UMTM, warp yarn shows a high breaking stress of 140.6 MPa and a breaking strain of 38.4% (Figure 2h). It is worth mentioning that the polymerization and crystallinity of viscose for inner weft yarn is smaller than cotton, thus it has a higher breaking strain than the cotton fibers (Figure S6, Supporting Information). In addition, the HIWY, SOWY, and WTWY are fine, mass-productive, low-cost, and skin-friendly, showing great potential in functional and smart textiles (Figure 2j).

2.2. UWTM Weaving and Unidirectional Water Transportation Performance

To systematically study on the weaving structure on the unidirectional moisture transportation property, six kinds of UWTM with different weaving lifting patterns and yarn properties were fabricated using semi-automatic loom, as illustrated in Figure 1a, **Figure 3** and Video S1, Supporting Information. 2D satin-weave (Figure 3a), weft-double–weave (Figure 3b), and stitching-double–weave structures (Figure 3) are reasonable designed and named as 1#, 2#, and 3#. The fabric weaving pattern, fabric front, and back surface, diagrams, and optical microscope photos of the three types of fabrics are shown in Figure 3. The transverse yarns are weft yarns, and the longitudinal yarns are warp yarns. For each weave structure, two kinds of weft yarn sets are used, and the prepared samples are named as (i) and (ii). The specific yarn configuration for each sample is shown in Table S1, Supporting Information. As shown in Figure 3a,c, the structure of the metafabric allows the adjacent weft yarns to line up on both sides of the fabric under the action of the weft beating force. Thus, both sides of the fabric show hydrophilic (HIWY dominant) and hydrophobic (SOWY dominant) weft weave points, respectively. As shown in Figure 3b, the hydrophilic surface of the fabric mainly presents HIWY weave points, in contrast to its hydrophobic surface, which is mainly composed of SOWY weave points. To better illustrate the hydrophilicity difference between the yarns, a dyeing process in conducted on the three kinds of fabrics. The hydrophilic yarns in Figure 3 show blue color while the hydrophobic yarns kept as white. Among the three designs, 2D satin-weave is formed by a set of warp yarns interwoven with a set of weft yarns, thus hydrophilic points can be observed on the hydrophobic surface, which can enhance the speed of single guide water but also allow the water diffusion. Weft-double-weave and stitching -double-weave are formed by interweaving two sets of weft yarns with one set of warp yarns, and with two sets of warp yarns. The former, one group of warp yarns shows faster water conductivity. And the latter, two groups of warp yarns make the interface between the two layers of the fabric clearer. Weft-double–weave and stitching-double–weave are double-layer fabrics with a smaller weft density, to achieve a thickness like that of a single-layer fabric with satin weave structure. Therefore, it is obvious to notice the pores on the surface of the fabric, which helps to enhance the capillary effect. At the same time, there is a lower layer of yarns below the pores, and when the water droplets stay on the surface of the fabric, these underlying yarns can provide the force for the droplets. In the fabric back side images and the fabric schematic (Figure 3), hydrophilic points can be observed on the main hydrophobic surface, where a hydrophilic yarn is added every two weaving cycles to enhance the unidirectional water transport ability of weft-double-weave and stitching-double-weave. This can be clearly drawn from the arrow points on the optical microscope photographs of the fabric in Figure 3. With weaving technology, microfluidic channels can be programmable designed and integrated into fabrics.

Figure 4a shows the weaving process of UWTM. First, the weave charts for three weaving patterns are designed and input into the computer software. Then, the warp yarns are guided to pass through the herald frames, reed, and then fixed on the warp beams (Figure 1b). Afterward, the weft yarns are fed into the loom regularly at intervals and interlaced with the warp yarns by tapping the fabrics using reed. The process is mass-productive, controllable, and rich in designing patterns.

A moisture management tester (MMT) was utilized to characterize the directional water transport performance quantitatively. The optical images in Figure 4b presents the water content on the top and bottom surface of three kinds of UWTMs where 2 μL water was dropped on the hydrophobic surface (top surface). When dropping water on the hydrophobic layer, the

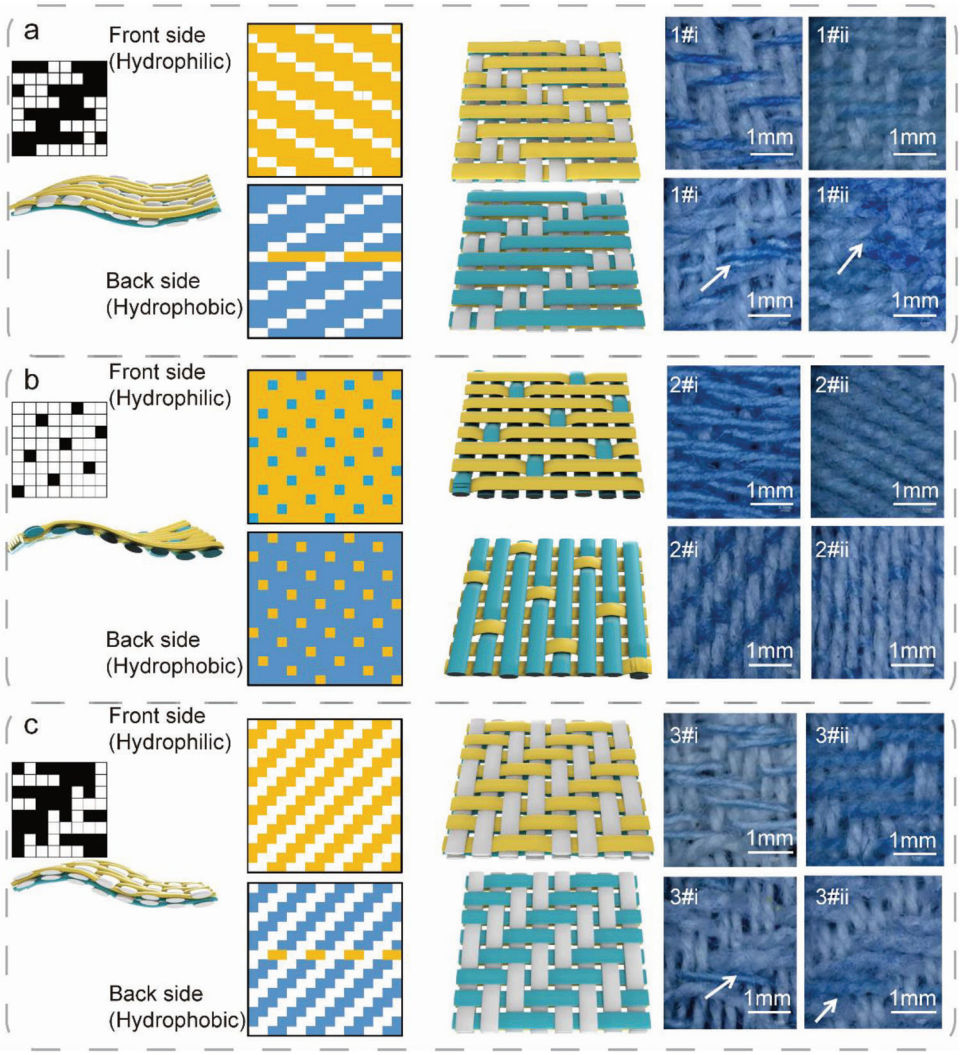

Figure 3. Programmable weaving patterns with architected microfluidic channels for unidirectional water transportation fabrics. Fabric weave chart, fabric front/back side, schematics, and optical microscope photos of a) weft-double–weave, b) satin-weave, and c) stitching-double–weave fabrics. Yellow stripes are hydrophilic yarn, white stripes are PET yarns, and blue stripes are superhydrophobic PET yarns. To observe the surface structure of the fabric more clearly, fabrics were dyed into blue color. In the optical images, the arrows at fabric backside are the hydrophilic yarns interlaced into hydrophobic side to accelerate the water droplet transportation.

water content on the bottom surface (hydrophilic layer) increased rapidly, and the wetting time of the bottom surface was ≈2 s. The hydrophobic layer stayed around zero except a small increase, which proves that water absorption is almost no water absorption on hydrophobic layer. This is because the stronger capillary force (F_C)of hydrophilic layer, which extracted the water from the hydrophobic layer to hydrophilic layer. Among three UWTMs, weft-double–weave fabrics (1#) shows best unidirectional water transport capacity than other two weave because of the Janus and hierarchical structure design. One set of warp yarn and the two sets of weft yarn can ensure a certain distance between hydrophobic layer and hydrophilic layer, but also can accelerate the moisture transfer through the warp yarn. Interestingly, although UWTM woven fabrics are thicker than conventional one-way water transport fabrics, the moisture transmission speed of our UWTM reaches 0.67 mm s^{-1}, which is higher than 0.50 mm s^{-1} of cotton textile fabricated by graphene oxide coatings,[12] 0.37 mm s^{-1} of porous Murray membranes prepared by electrostatic spinning[1d] and 0.33 mm s^{-1} of orthogonal woven fabric.[1e] Also, the wetting time of cotton fabrics (ii) is slower than those of viscose fabrics (i). Strong wettability of viscose yarn allows viscose fabrics to exhibit faster unidirectional water transport rates. As a result, although water could enter the fabric easily, it would be trapped in the fabric, thus, wetting areas are also larger.

Figure S7a, Supporting Information, shows the accumulative water transport capacity (R) of the fabric. Among them, weft-double–weave fabrics (1#) show the highest capacity of more than 960%, demonstrating an outstanding unidirectional water transmission ability. The 2D single-layer fabrics (2#) are interwoven by a set of warp and weft yarn system, but the interlacing of hydrophilic and hydrophobic yarns causes the interface

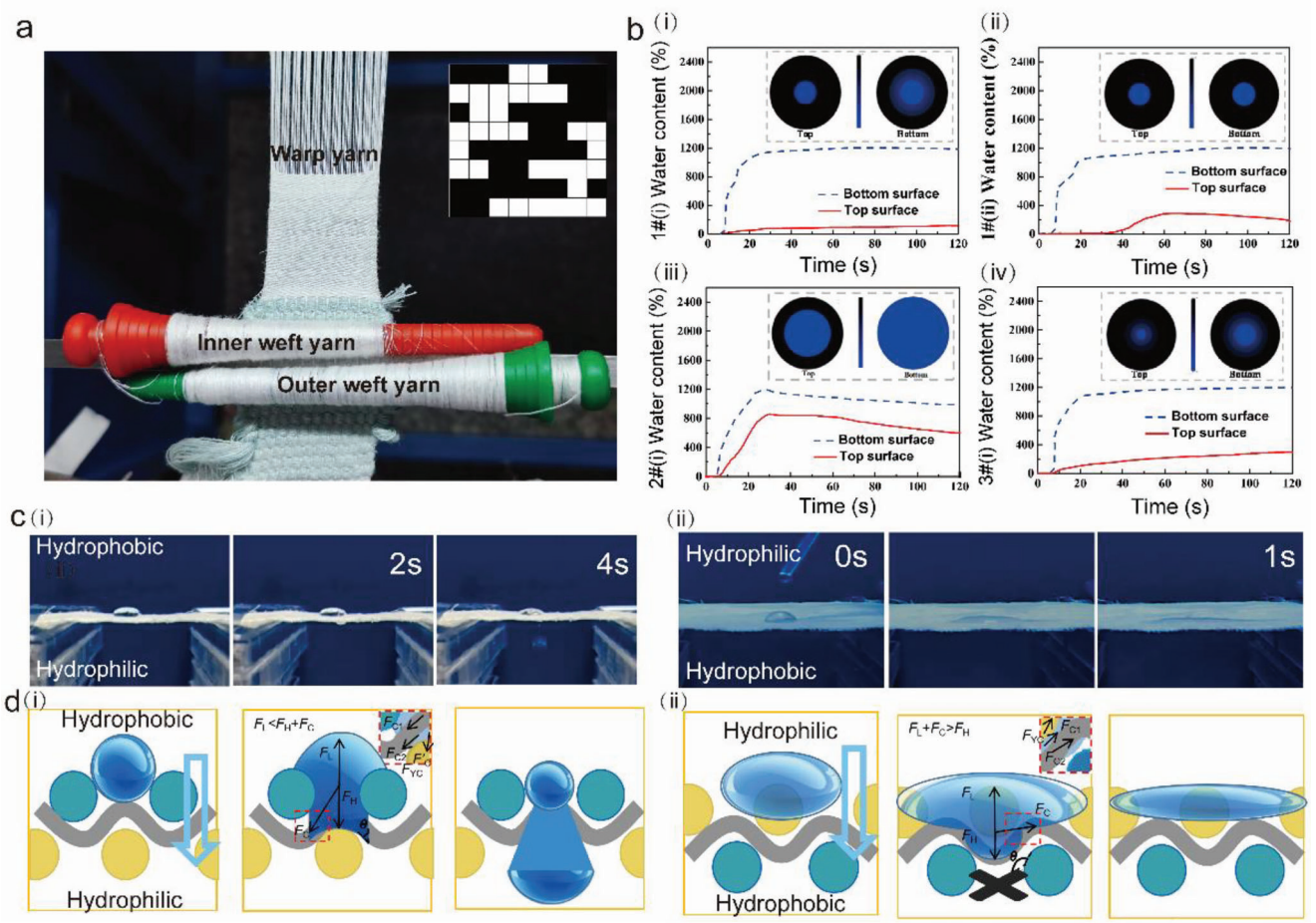

Figure 4. UWTM weaving and the unidirectional water transportation mechanism. a) Weaving process of the weft-double-weave fabric, with two sets of weft yarns and one set of warp yarn. Inset is the lifting pattern plan for the weft yarn. b) Moisture management test of weft-double–weave with i) viscose and ii) cotton yarns as the inner weft yarn, iii) satin-weave and iv) stitching-double–weave with viscose as inner weft yarn. c) Real-time i) penetration process when 2 µL water drops on hydrophobic surface of the UMTM, and ii) diffusion process when it is on hydrophilic surface, showing an obvious unidirectional water transportation property. d) Mechanism of the unidirectional water transport.

between hydrophobic and hydrophilic layers to be relatively ambiguous, which results in no ideal difference in wettability gradient and affects the efficiency of water transport capacity. The UWTM with two sets of yarn system of the double fabric solve the above problem, so its capacity is higher. The hydrophilic yarn on the main hydrophobic surface of the double-layer fabric works as a diversion, which enables the rapid transfer of liquid to the main hydrophilic surface. Simultaneously, the proper hydrophilic/hydrophobic area ratio keeps the main hydrophobic surface dry and contributes to maintaining a comfortable dressing experience.

2.3. Unidirectional Water Transportation Mechanism and Microfluidic Dynamics for UWTM

Figure 4c,d and Figure S8, Supporting Information, illustrates the unidirectional water transportation mechanism for the satin-weave, weft-backed–weave, and stitching-double–weave fabrics. If the droplet is on the hydrophobic side, it will penetrate quickly from the hydrophobic layer to the hydrophilic layer due to the water droplet hydraulic force (F_H) caused by the gravity of those droplets, as shown in Figure 4c(i) and Video S2, Supporting Information. If water droplet is on the hydrophilic side, the liquid can only spread on the hydrophilic side since it will be resisted by the hydrophobic yarn, as shown in Figure 4c(ii) and Video S3, Supporting Information. In Figure 4de, F_L is the Laplace force, generated by the difference in pressure inside and outside the liquid due to the presence of the curved liquid surface. F_C is the capillary force, generated by the capillary force of the HIWY (F_{YC}), the capillary force of the pores between the yarns (F_{C1}) and the wicking force of the WTWY (F_{C2}). When the water droplets in the pores are in close contact with the hydrophilic side, the hydrophilic side has a F_C and F_L on the droplets, the liquid droplets will be "dragged" to the hydrophilic side, realizing the penetration of the liquid to the fabric. Therefore, the hydrophilic/hydrophobic fabrics are also called "liquid diode,"[13] where liquids can only be transported from the hydrophobic side to the hydrophobic side. The diffusion and penetration phenomena of droplets on satin-weave fabric (Figure S7a, Supporting Information) are

relatively simple due to short transport paths. The penetration path of droplets is mainly the pores between hydrophobic yarns, and the diffusion path is hydrophilic yarns and pores between yarns. In the thickness direction, it forms a wettability gradient from hydrophobic layer to hydrophilic layer. In the hydrophobic surface of weft-double–weave fabric (Figure S7b, Supporting Information, and Figure 3a) and stitching-double-weave fabric (Figure S7c, Supporting Information), hydrophilic yarns are regularly added to enhance the efficiency of water transport. Meanwhile, the multiple warp and weft yarns system also makes the path of droplet transport more complicated. In the penetration process, most of the droplets will penetrate to the hydrophilic side through the gaps between the hydrophobic yarns, while a few droplets will transfer directly to the hydrophilic side through the hydrophilic yarns on the hydrophobic surface. In the diffusion process, droplets will spread rapidly along the hydrophilic yarns on the hydrophilic side and will not penetrate under the F_L. Both fabrics formed a wettability gradient in the thickness direction. The former is from hydrophobic layer, liquid transport layer to hydrophilic layer, while the latter is hydrophobic layer, two liquid transport layers to hydrophilic layer. Overall, the wettability gradient of the weft-backed fabric was more uniform and consistent, which results in better unidirectional water transport function. In summary, weft-backed–weave fabric 1# has the best unidirectional water transport performance among the three kinds of fabrics. Video S4, Supporting Information, shows the weft-backed–weave fabric made of interwoven polyester yarns and viscose yarns without superhydrophobic treatment. When water droplet touches the super hydrophobic side, the droplet quickly spread on the surface of the fabric without transferring to the hydrophilic side. It is proved that the untreated weft-backed–weave fabric does not have the properties of unidirectional water transport function.

As shown in Figure 4d(i), when the droplet drops onto the hydrophobic side, the droplet forms a curved liquid surface on the lower surface of the pores on the hydrophobic side. Precisely the presence of the curved liquid surface causes the difference in pressure between the inside and outside of the liquid, generating F_L. The F_L is opposite to the F_H direction. The F_L relationship is $F_L = -2\gamma_{LV}/r$, where γ_{LV} is the tension at the gas/liquid interface and r is the radius of the liquid bend surface.[14] Meanwhile, the yarn exerts a downward F_C on the droplet. F_C can be subdivided into F_{YC} (dominant role) due to wetting and pore formation of hydrophilic yarn itself, F_{C1} due to pore space between yarns, and F_{C2} due to water transport yarn. When the curved liquid surface of the liquid is in contact with the hydrophilic layer due to the F_C of the hydrophilic layer, the gas/liquid interface will be destroyed, which leads to the reduction of the F_L, at which time $F_L < F_C + F_H$. Then the liquid can diffuse on the hydrophobic layer and penetrate the Janus fabric to the hydrophilic side of the fabric, realizing the directional movement of the liquid. When there is hydrophilic yarn on the hydrophobic side, it will increase the F_C and promote more rapid penetration of liquid droplets.

To achieve the above behavior when the fabric interacts with the liquid, three conditions are required. One, the two sides of an anisotropic fabric require an opposite wettability, as described above. Two, there should be a certain distance between hydrophilic layer and hydrophobic layer, and reasonable control of the distance between the two, so that the F_L exists and as small as possible. Three, the liquid needs to act on the hydrophobic side of the fabric.

As shown in Figure 4d(ii), when a water droplet drops onto the hydrophilic side of the fabric, the droplet first diffuses to form a thin liquid film on the hydrophilic side, and then is blocked at the hydrophobic/hydrophilic interface. At this point, there is a combination of F_L, F_H, and F_C on the liquid surface. By further increasing F_H, the liquid will form a curved liquid surface below the lower hydrophobic membrane pores until the sum of the maximum F_L and F_C is reached, and then the liquid can penetrate the fabric. Under normal circumstances, the sum of F_L and F_C is much greater than the F_H, so when the liquid acts on the hydrophilic side of the Janus fabric, the liquid can only diffuse on the hydrophilic side.

Figure 4c shows the penetration process of 2 µL drop on UWTM hydrophobic surface and the diffusion process of hydrophilic surface with sample 1#(i). The asymmetric wettability makes the differential capillary effect on both sides of the fabric, which realizes the water transfer on one side. When water droplet drops onto the main hydrophobic surface, water droplets do not spread under low surface tension, but are dragged by the F_C and penetrate the fabric quickly. When the water droplet drops onto the main hydrophilic surface, water droplet spreading occurs under the action of high surface tension in the hydrophilic layer, wicking occurs under the F_C. When it meets hydrophobic substances, the hydrophobic resistance prevents its penetration, thus only diffusing occurs.

The water transport performance is characterized by wicking height and wicking speed inside the fabric during water absorption, which is influenced by the capillary pressure.[15] Capillary force is related to the capillary equivalent radius, the gas/liquid surface tension, and the cosine of the contact angle.[16]

$$F_C = \frac{2\gamma_{LV}\cos\theta}{\bar{r}} \quad (1)$$

where Fc is the capillary force. $\bar{r}$, θ, and γ_{LV} represent the equivalent radius of the capillaries, the water contact angle of the fabric, and the surface tension of the liquid, respectively. As shown in **Figure 5**a, when the contact angle between the fabric and the liquid is less than 90°, positive wicking will occur, indicating water conductivity (as shown in Figure 4d(i), $F_L < F_H + F_C$), and conversely, water repellency (as shown in Figure 4d(ii), $F_L + F_C > F_H$). Therefore, wicking height can be divided into positive wicking and negative wicking, and the corresponding water conductivity height and water repellency height of the fabric is the comprehensive expression of the water transport performance of the fabric, respectively.[17]

As shown in Figure 5b, wicking rate of the fabric is faster in the initial stage, which is due to the combined effect of the hydrophilicity of the yarn itself and the capillary effect caused by the pores between the fabrics. The F_C is influenced by the fabric weave structure[18] and surface wettability.[19] As the water content increases, the hydrophilic groups on viscose and cotton absorb a large amount of direct water and indirectly water.[20] The water makes the pores between the yarn and the fabric gradually block, and the F_C decreases. Eventually, the wicking height reaches a stable value under the action of gravity.

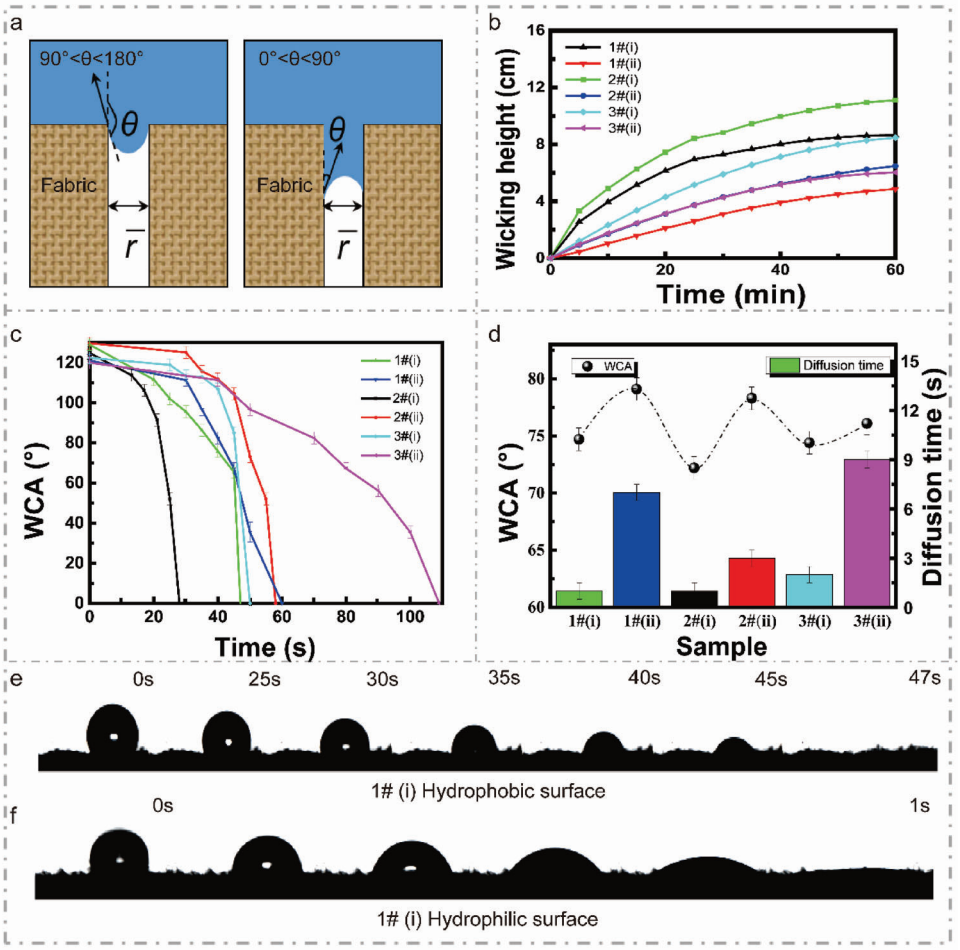

Figure 5. Microfluidic dynamics of UWTM. a) Wicking model for fabrics with positive and negative wetting. b) Wicking height of 1#) weft-double–weave, 2#) satin-weave, and 3#) stitching-double–weave structures using i) viscose and ii) cotton as inner weft yarns. c) Dynamic contact angle for the fabrics when droplets on the hydrophobic surface. d) Contact angle and diffusion time of water on the hydrophilic surface. e) and f) Real-time images of the droplet movement on both sides of the UWTM.

The wicking height of viscose fabric (i) is higher than that of cotton fabric (ii) of the same fabric weave. This is because viscose owns a lot of microgrooves on the fiber surface with a large specific surface area. Moreover, the crystallinity of viscose is lower than that of cotton, resulting in a better water absorbency.[21] Besides, the wicking height of single-layer fabric (2#) is higher than that of double-layer fabric (1# and 3#), which is due to single layer fabrics have only one warp and weft yarn system and the yarns are closely aligned with each other. Satin-weave has a longer floating length line accompanied by plenty of capillary paths between yarns. The liquid is driven by the wicking force of the fabric, overcoming gravity to climb upward. The two layers of weft-double–weave (i and ii) share the same set of polyester warp yarns, which exhibit superior wicking performance in double-layer fabrics.

Figure 5c exhibits that the water contact angle (WCA) of six fabrics can reach more than 120° on the hydrophobic surface, demonstrating good hydrophobicity. The contact angle becomes progressively smaller as the water droplets exist on the hydrophobic surface for an extended period. The Laplacian force (F_L) and hydraulic force (F_H) act on the solid/liquid interface when the droplet drops to the hydrophobic surface. With the extension of time, the liquid will form a bent liquid surface below the lower hydrophobic surface pores. When the bend liquid surface touches the hydrophilic surface yarn, it will be destroyed, and F_L will drop sharply. At the same time, under the F_C of the hydrophilic surface, the liquid can penetrate from the hydrophobic surface to the hydrophilic surface, completing the process of unidirectional penetration.[22] Therefore, the WCA of the hydrophobic surface changes very little for a long time in the initial stage. When the Laplace pressure on the droplet surface decreases sharply, it will be accompanied by rapid penetration (Figure 5c). The instantaneous WCA of the hydrophilic surface of six fabrics is below 80°, and the droplet diffusion time on the hydrophilic surface is within 10 s, reflecting the good wettability of the hydrophilic surface (Figure 5d).

Figure 5e,f shows the difference in wettability on both sides of the fabric makeing the gravity of the droplet and the wicking force of the hydrophilic fabric larger than F_L on the hydrophobic surface of the fabric, which makes the liquid penetrate through the hydrophobic surface of the fabric. On the contrary, water droplets do not penetrate the hydrophilic surface but spread along the surface of the fabric and reach diffusion

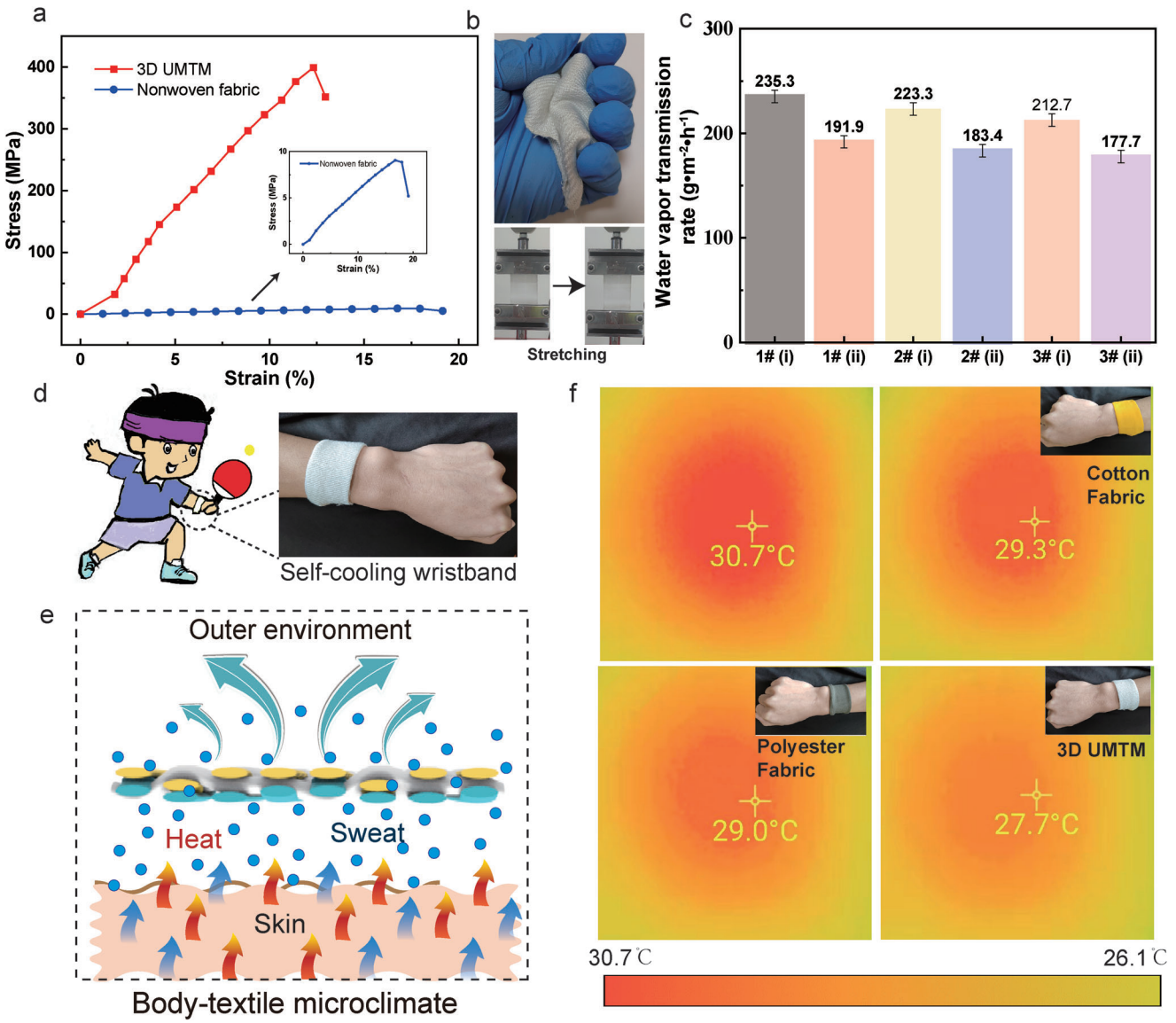

Figure 6. UWTM for wearable evaporative cooling. a) Mechanical performance of UWTM and a commercial nonwoven fabric. UWTM shows a robust mechanical property with a high breaking strength of 400 MPa, while nonwoven fabric exhibits a weak mechanical property. b) Flexibility and stretchability of the UWTM. c) Moisture transmission rate of UWTM. All three UWTMs show a good moisture transmission property. d) Application of UWTM to self-cooling wristband. e) Human body-textile microclimate for maintaining body comfort during exercise. f) Infrared image showing temperature different between UWTM and conventional textiles, including cotton fabrics and polyester fabrics. UWTM showing a distinguishing cooling performance.

equilibrium within 1 s. The reason is that F_H is not sufficient to overcome the combined effect of F_L and F_C. Therefore, the perspiration on human skin will penetrate from human body to the outer side of the textile, then evaporate into the atmosphere, but the water droplet cannot reversely pass-through UMTM to human skin.

2.4. UWTM for Evaporative Cooling

The textiles arising from the water responsiveness has a wider application prospect in the field of personal conditioning textiles, such as wristbands, hair bands, and insoles. When controlling other factors constant, the excessive moisture can be absorbed and transferred from one side to the other side due to the unidirectional water transport.[23] To meet the requirements for wearable clothes, textile should have a robust mechanical property. However, current textiles for unidirectional sweat transportation are mostly nonwovens, which is normally lack of mechanical strength. In our work, UWTM shows a high breaking stress of near 400 MPa, which is much higher than normal PET nonwoven textiles, as demonstrated in **Figure 6**a. The excellent mechanical property ensures the good property to withstand the daily abrasion, stretching, and wash rubbing. Therefore, compared to nonwoven based sweat wicking textiles, UWTM shows greater potentials for wearable applications. In

addition, UWTM is stretchable, flexible, bendable, and conformable (Figure 6b). Moreover, UWTM also shows a high moisture transmission property (Figure 6c), which is indispensable to guarantee the wearing comfort.

UWTM is further developed into a smart wristband with passive cooling ability to maintain a wearing body-textile microclimate in hot situations, as shown in Figure 6d,e. To imitate the process of human sweating under hot environment, 2 μL of 36 °C water drops were placed on the wrist of the tester. After 30 s, the temperature on the fabric surface is detected using thermal camera. Figure 6 shows the infrared images of the wrist while wearing UWTM and other commonly used textiles, such as cotton fabric and polyester fabrics. It is clearly shown that the UWTM has distinctive functionality of cooling (27.7 °C) upon contact with the heat source (36 °C) and the temperature decreased by 1.3 and 1.5 °C compared with cotton fabric and polyester fabric, respectively. The underlying cause could be that sweat is transported and diffused into the outer hydrophilic layer of the UWTM, speeding up evaporation and taking away excess heat. Hence, the UWTM can be widely used in functional textiles for outdoor sports to maintain human thermal and wet comfort.

The air permeability of fabric is a key index to evaluate the comfort degree of functional textiles. Therefore, we supplemented the air permeability comparison experiment of untreated and treated polyester, and viscose yarns interwoven fabrics, the test standard based on GBT5453-1997 textile fabric breathability determination. As shown in Figure S9, Supporting Information, both pristine fabrics and weft-double–weave fabrics (1#) demonstrate good air permeability, which is 327.93 and 258.07 mm^{-1} respectively. The slight decrease of the treated fabric is mainly caused by the obstruction of the fabric pores owing to the co-MBAA-DVB nanoparticles attached to the surface of the hydrophobic polyester yarns, which resulted in the disappearance of some tiny pores between the yarns. This result shows that the unidirectional water transportation fabric still exhibits good breathability and comfort in wearable applications. The combination of proper air permeability and excellent unidirectional water-transportation will greatly extend the range of applications of versatile textiles. In addition, the water washing resistance of fabrics is also one of the important characteristics for long-term wearing. As shown in Figure S10, Supporting Information, after one washing cycle, the adhesion of co-MBAA-DVB on the fabric surface does not decrease significantly, which can also be seen from its surface wettability, and the fabric still has the feature of superhydrophobic (WCA is 151°). After five washing cycles, the adhesion of co-MBAA-DVB on the fabric surface decreased gradually with the increase of washing times, but they are still evenly distributed on the yarns, giving the yarns a certain roughness, resulting in a hydrophobic effect of the fabric (WCA is 145.7°), and forming a Janus wettability gradient with the hydrophilic side. Therefore, the unidirectional water transfer characteristics of UWTM are potentially stable after different washing cycles.

Besides the evaporative cooling effect, UWTW can also work as a radiative emitting textile because of the high emissivity in the mid infrared wavelength range, as shown in Figure S11, Supporting Information. The textile can radiate heat to the atmosphere, which normally has a lower temperature than human skin. Therefore, when human skin sweat, the evaporative cooling will dominate the cooling; when the textile gets fully dried, the radiative cooling will take the main role for cooling. This enables UWTM work as a dual-mode cooling textile.

3. Conclusion

In this work, a hierarchical weaving metafabric is developed for unidirectional sweat transportation and passive cooling. The UWTM is fabricated using three kinds of yarns with wettability gradient by an industrialized weaving technology. Through reasonable hydrophobic finishing and fiber surface engineering, the outer weft yarn, water transportation warp yarn, and inner weft yarn exhibit a water contact angle of 159.7°, 112.2°, and 26.1°, respectively, forming an excellent wettability gradient. Meanwhile, the three yarns show a robust mechanical property, which guarantees the further weaving process under tension. The UWTM shows a strong one-way transport capacity of 984.01%, with a short water droplet transportation time of 4 s. In addition, the unidirectional water transportation leads to an evaporative cooling effect to the human body, resulting in a 1.6 °C cooling compared with the most used cotton fabrics, exhibiting excellent wet-heat transfer responsiveness, and ensuring a comfortable temperature and humidity for the human body. The facile and scalable method presented here paves the way for the design of fluorine-free, comfortable, and wearable unidirectional water transport fabrics. In addition, programmable open microfluidics in textiles is demonstrated through the architected design of yarn hydrophilicity, morphology, and weaving density, providing wide application prospects not only in personal thermoregulation, but also in microfluidics such as liquid handling, wearable diagnostic devices.

4. Experimental Section

Materials: Polyester yarn and raw cotton yarn were provided by Star Textile Accessories Co. (China). Viscose yarn was provided by Fujian Xinhuayuan Textile Co. (China). Osmotic agent (JFC) was provided by Jinan Yunhai Chemical Co. (China). Sodium hydroxide (NaOH), acetone, MBAA, DVB, azodiisobutyronitrile (AIBN), vinyltrimethoxysilane, PDMS, and ethyl acetate were provided by Aladdin's Reagent Shanghai Co. (China).

Preparation of Superhydrophobic Polyester Yarn: DVB was synthesized into PDVB by in situ polymerization method. AIBN was used as initiator, MBAA and DVB mixture was used as solvent. AIBN, MBAA, and DVB were dissolved in the DMF solution for 60 min with an oscillator at 120 r min^{-1}. The synthesis kettle was then placed in a vacuum oven at a temperature of 100 °C for 24 h and then removed. The solution was dried and ground to obtain co-MBAA-DVB.

co-MBAA-DVB, PDMS, and α-cyanoacrylate were fully dissolved in ethyl acetate solution in a certain proportion. The hydrophobic solution was obtained by ultrasonic shaking for 20 min. Then, the polyester yarns (polyester A) were soaked in a hydrophobic solution for 10 min, followed by drying to move the solution of ethyl acetate. Finally, polyester yarns were treated via the plasma technique in vacuum to obtain superhydrophobic polyester yarns (polyester B).

Preparation of Modified Cotton Yarn: The cotton yarn was treated to remove the natural gums and waxes remaining on its surface. First, the original cotton yarn was rinsed with acetone and then rinsed three times with deionized water. Second, the impurities on the cotton yarn were removed by dissolving NaOH and JFC at 2% and 3% in deionized water to

configure the pretreatment solution. The yarn was soaked in solution for 30 min at 90 °C. Finally, the yarn was washed and dried to obtain alkali-treated cotton yarn.

Weaving of UWTM: SGA598 semi-automatic loom was used for weaving. The weaving process of fabric was divided into four steps: heald, reed, warping, and weft beating. Two shuttles were needed for double fabric because the front and back sides show different effects. Satin-weave, weft-double–weave, and weft-double–weave were fabricated to investigate the effect of fabric structure on the OWT properties. The detailed yarn configuration of three kinds of weaved fabrics is shown in Table S1, Supporting Information. Thickness of woven fabrics can be manipulated by reasonable weft density control. Warp density of fabric was 248 yarns per 10 cm. Weft density of single-layer fabric was larger to guarantee the thickness of single-layer fabric close to double-layer fabric. Meanwhile, a hydrophilic yarn was added to the main hydrophobic surface of the double-layer fabric every two organizations to improve OWT performance of the fabric.

Fabric Comfort and Water Resistance Test: Air permeability test: the test standard based on GB/T5453-1997 textile fabric breathability determination. According to the breathability standard of the textile, the applied pressure was 100 Pa, the applied area was 20 cm^2, and the air permeability of the fabric was measured ten times at different positions to take the average value.

Washing process: Fabric size: 2×2 cm^2. 0.3% laundry liquid was added into 100 mL deionized water and prepared it into washing solution. The fabric was soaked in the washing liquid and stirred magnetically for 20 min at 40 °C and 120 r min^{-1}, and then dried in an oven at 80 °C for 10 min. The above operation was regarded as a washing cycle, and a total of five washing cycles were carried out. The surface morphology and adhesion of superhydrophobic particles were observed by SEM of the fabric after five washing cycles.

Characterization of Unidirectional Water Transportation: The surface morphology of the yarns was characterized by optical microscope, SEM, and Nicolet6700 Fourier transform infrared measuring instrument. The mechanical properties of yarn were characterized by yarn strength and elongation tester. The wicking height of yarn and fabric was measured by YG (B) 871 capillary effect tester. The fabric contact angle was measured by contact angle tester. M290 MMT liquid water management tester was used to measure unidirectional water transport capacity based on the GB/T21655.2-2019 standard. Shooting device was used to film the process of single guide wetting of fabrics. The process of moisture absorption and heat conduction of fabrics was captured by T3 Pro thermal imager.

Informed Consent: The volunteer (Ling Zhang) agreed to all tests in the manuscript with informed consent.

Supporting Information

Supporting Information is available from the Wiley Online Library or from the author.

Acknowledgements

This work was supported by the National Key R&D Program of China (2016YFC0802802).

Conflict of Interest

The authors declare no conflict of interest.

Data Availability Statement

The data that support the findings of this study are available from the corresponding author upon reasonable request.

Keywords

asymmetric wettability, evaporative cooling, superhydrophobicity, unidirectional water transportation, weaving metafabric

Received: July 4, 2023
Published online:

[1] a) C. Zeng, H. Wang, H. Zhou, T. Lin, *Adv. Mater. Interfaces* **2016**, *3*, 1600036; b) L. Hou, J. Liu, D. Li, Y. Gao, Y. Wang, R. Hu, W. Ren, S. Xie, Z. Cui, N. Wang, *Chem. Res. Chin. Univ.* **2021**, *37*, 337; c) X. Jinhao, Z. Fuli, X. Binjie, W. Chun, Y. Dan, Z. Yuansheng, Z. Mengjuan, *Polym. Adv. Technol.* **2019**, *30*, 3038; d) X. Wang, Z. Huang, D. Miao, J. Zhao, J. Yu, B. Ding, *ACS Nano* **2019**, *13*, 1060; e) W. Fan, G. Zhang, X. Zhang, K. Dong, X. Liang, W. Chen, L. Yu, Y. Zhang, *Small* **2022**, *18*, 2107150; f) Y. Wang, Z. Wang, Z. Lu, M. J. de Andrade, S. Fang, Z. Zhang, J. Wu, R. H. Baughman, *ACS Appl. Mater. Interfaces* **2021**, *13*, 6642.

[2] a) Y. Dong, J. Kong, S. L. Phua, C. Zhao, N. L. Thomas, X. Lu, *ACS Appl. Mater. Interfaces* **2014**, *6*, 14087; b) Y. Peng, H. K. Lee, D. S. Wu, Y. Cui, *Engineer* **2022**, *10*, 167; c) Y. Peng, W. Li, B. Liu, W. Jin, J. Schaadt, J. Tang, G. Zhou, G. Wang, J. Zhou, C. Zhang, Y. Zhu, W. Huang, T. Wu, K. E. Goodson, C. Dames, R. Prasher, S. Fan, Y. Cui, *Nat. Commun.* **2021**, *12*, 6122; d) R. Wang, S. Fang, Y. Xiao, E. Gao, N. Jiang, Y. Li, L. Mou, Y. Shen, W. Zhao, S. Li, A. F. Fonseca, D. S. Galvão, M. Chen, W. He, K. Yu, H. Lu, X. Wang, D. Qian, A. E. Aliev, N. Li, C. S. Haines, Z. Liu, J. Mu, Z. Wang, S. Yin, M. D. Lima, B. An, X. Zhou, Z. Liu, R. H. Baughman, *Science* **2019**, *366*, 216; e) R. Wu, J. Bae, H. Jeon, T. Kim, *Chem. Eng. J.* **2022**, *444*, 136556.

[3] S. Okubayashi, U. J. Griesser, T. Bechtold, *J. Appl. Polym. Sci.* **2005**, *97*, 1621.

[4] a) R. Bagherzadeh, M. Gorji, M. Latifi, P. Payvandy, L. X. Kong, *Fibers Polym.* **2012**, *13*, 529; b) E. Onofrei, A. M. Rocha, A. Catarino, *J. Ind. Text.* **2012**, *42*, 34.

[5] X. Dai, N. Sun, S. O. Nielsen, B. B. Stogin, J. Wang, S. Yang, T.-S. Wong, *Sci. Adv.* **2018**, *4*, eaaq0919.

[6] X. Tian, H. Jin, J. Sainio, R. H. A. Ras, O. Ikkala, *Adv. Funct. Mater.* **2014**, *24*, 6023.

[7] K. A. McCulloh, J. S. Sperry, F. R. Adler, *Nature* **2003**, *421*, 939.

[8] H. Wang, H. Zhou, X. Wei, H. Niu, T. Lin, *Adv. Mater. Interfaces* **2018**, *5*, 1800815.

[9] H. Wang, H. Zhou, H. Niu, J. Zhang, Y. Du, T. Lin, *Adv. Mater. Interfaces* **2015**, *2*, 1400506.

[10] M. Zhang, Q. Yang, M. Gao, N. Zhou, J. Shi, W. Jiang, *J. Environ. Chem. Eng.* **2021**, *9*, 106016.

[11] L. Ma, R. Wu, A. Patil, S. Zhu, Z. Meng, H. Meng, C. Hou, Y. Zhang, Q. Liu, R. Yu, J. Wang, N. Lin, X. Y. Liu, *Adv. Funct. Mater.* **2019**, *29*, 1904549.

[12] X. Guan, X. Wang, Y. Huang, L. Zhao, X. Sun, H. Owens, J. Lu, X. Liu, *Adv. Mater. Interfaces* **2020**, *8*, 2001427.

[13] S. Ruilin, Y. Ling, L. Liangzhong, C. Da, L. Hai, F. Xiaoyun, L. Guoqiang, M. Ruixue, A. Kun, Y. Yang, *Sep. Purif. Technol.* **2021**, *277*, 119423.

[14] Z. Zhihong, N. Yuzhen, B. Shuang, Z. Xudong, L. Qiang, Y. Cunming, J. Xu, L. Kesong, J. Lei, *Adv. Sci.* **2021**, *9*, 2103765.

[15] Y. Zheng, Y. Chen, G. Fei, J. Dorsey, E. Wu, *IEEE Trans. Vis. Comput. Graph.* **2019**, *25*, 2471.

[16] a) R. N. Wenzel, *Ind. Eng. Chem.* **1936**, *28*, 988; b) A. B. D. Cassie, S. Baxter, *Trans. Faraday Soc.* **1944**, *40*, 546; c) A. Tuteja, W. Choi, M. Ma, J. M. Mabry, S. A. Mazzella, G. C. Rutledge, G. H. McKinley, R. E. Cohen, *Science* **2007**, *318*, 1618.

[17] H. Almoughni, H. Gong, *Text. Res. J.* **2014**, *85*, 722.
[18] C. Zhu, H. Tada, J. Shi, J. Yan, H. Morikawa, *Text. Res. J.* **2019**, *89*, 5198.
[19] M. M. Garimella, S. Koppu, S. S. Kadlaskar, V. Pillutla, W. C. Abhijeet, *J. Colloid Interface Sci.* **2017**, *505*, 1065.
[20] E. Matyjas-Zgondek, K. Blus, E. Rybicki, *Fibres Text. East. Eur.* **2003**, *11*, 66.
[21] T. Kreze, S. Malej, *Text. Res. J.* **2003**, *73*, 675.
[22] L. Hou, N. Wang, X. Man, Z. Cui, J. Wu, J. Liu, S. Li, Y. Gao, D. Li, L. Jiang, Y. Zhao, *ACS Nano* **2019**, *13*, 4124.
[23] N. Li, L. Wu, C. Yu, H. Dai, T. Wang, Z. Dong, L. Jiang, *Adv. Mater.* **2018**, *30*, 1703838.